Supplementary material:Tollmien-Schlichting wave cancellation via localised heating elements in boundary layers

G. S. Brennan[1*] and J. S. B. Gajjar[1]† and R.E. Hewitt[1]

[1]Department of Mathematics, University of Manchester, Manchester, M13 9PL,UK

[*](current address):Mathematical Institute, University of Oxford, Oxford, OX2 6GG, UK

Supplementary material: Grid-size checks and wave packet behaviour

Whilst the results presented in the paper show excellent agreement with those predicted by the analytical solution especially for the Tollmien-Schlichting wave part of the signal, adequately resolving the downstream travelling wave packet part of the signal created many difficulties.

In figures 14-17 of the paper it can be observed that over the full range of X there is a wave packet with very large amplitude which develops ahead of the Tollmien-Schlichting wave and moves downstream. The same wave packet behaviour is present in computations both with and without localised heating, and as noted in the paper, only present for the pressure, displacement and velocity fields. However for the temperature perturbation shown in figure 12 no such wave packet is present.

In order to understand the nature of the wave packet behaviour grid size checks were performed. In all the figures we have confined our attention to the problem without localised heating. Also, the vibrator profile is taken to be the triangular hump shape $tr(X)$ of Terent'ev (1984)as defined in the paper. Initially the computations were performed over a much larger domain in Fourier (k) space, ($|k| \leqslant 40$) with a consequent greater spatial resolution in X.

In figure 1 we present results for the unstable case with $\omega = 2.5$ varying both the number of Fourier modes takes as well as varying the number of Chebychev points used in the Y direction. The results show fully spatially converged results even for the wave packet.

Next we investigated using different temporal schemes and varying the time-step. In the description of the numerical method only the second order fully implicit temporal differencing was described. However other schemes were also tried including the Crank-Nicolson scheme in which the equation

$$U_\tau + S(U) = R$$

is approximated by

$$\frac{U^{n+1} - U^n}{\Delta t} + \phi S(U^{n+1}) + (1-\phi)S(U^n) = R.$$

Taking $\phi = 1/2$ gives the Crank-Nicolson scheme, $\phi = 1$ gives the fully implicit scheme. In figures 1 the results show that as far as the restricted range of X is concerned the results obtained are the same across different schemes. However in figure 2, and figure 3 by changing the time-differencing scheme or using smaller time-steps, the wave packet

† Email address for correspondence: jitesh.gajjar@manchester.ac.uk

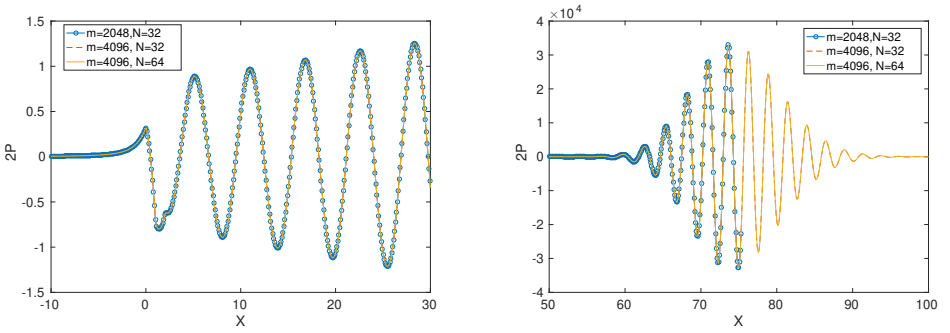

(a) (b)

Figure 1: Results for $\omega_0 = 2.5$ at $t = (K + \frac{1}{4})T_{period}, K = 8$ showing (a) the restricted X range and (b) the full computed range for different values of m the number of Fourier modes, and N the number of Chebychev modes.

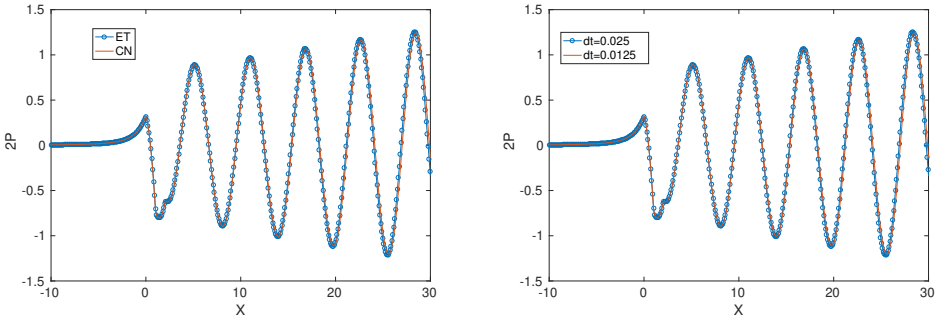

(a) (b)

Figure 2: Results for $\omega_0 = 2.5$ at $t = (K + \frac{1}{4})T_{period}, K = 8$.. The label ET denotes the scheme $\frac{3U^{n+1}-4U^n+U^{n-1}}{2\Delta t} + S(U^{n+1}) = R$ and the label Crank-Nicolson the scheme $\frac{U^{n+1}-U^n}{\Delta t} + \phi S(U^{n+1}) + (1-\phi)S(U^n) = R$ with $\phi = 1/2$.

behaviour is unresolved. In fact in figure 3 it can be seen that the amplitude of the wave packet increases as the time timestep is reduced.

It is clear from figures 3, 4 when looking at the full computed range, the results do not show convergence when using different time differencing schemes or when reducing the timesteps. In figure 5 we have compared results in using different functions $q(\tau) = 1-e^{-a\tau^2}$ with different values of a. Whilst these results show convergence in the restricted range of X, in the full computed range the amplitude of the wave packet depends on the value a. Although not shown in the results presented here, we additionally tried to initiate the temporal simulations at a time t_0 taking the asymptotic solution for small t_0 as the initial condition. However this did not make any difference to the results and behaviour described above.

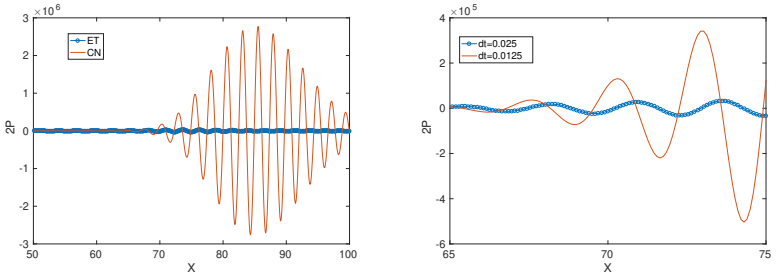

(a) (b)

Figure 3: Results for $\omega_0 = 2.5$ at $t = (K + \frac{1}{4})T_{period}, K = 8$. (a) The label ET denotes $\frac{3U^{n+1}-4U^n+U^{n-1}}{2\Delta t} + S(U^{n+1}) = R$. The label CN denotes $\frac{U^{n+1}-U^n}{\Delta t} + \phi S(U^{n+1}) + (1-\phi)S(U^n) = R$ with $\phi = 1/2$. In (b) results shown for different timesteps.

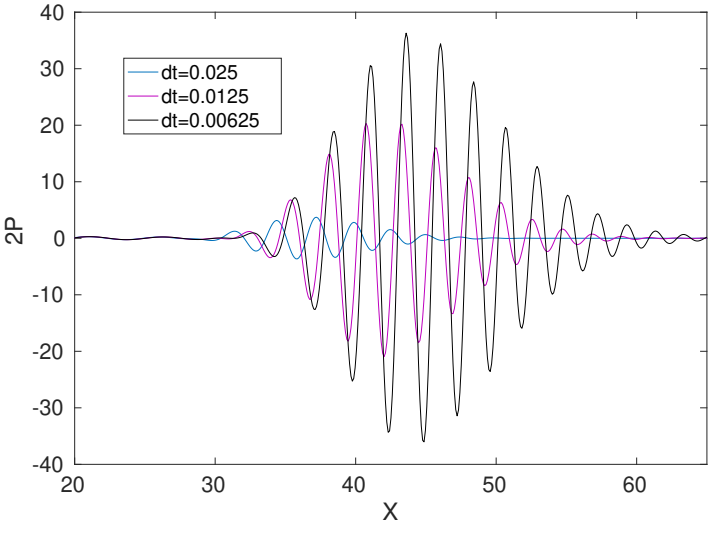

Figure 4: Results for $\omega_0 = 2.5$ at $t = (K + \frac{1}{4})T_{period}, K = 4$, for different timesteps dt.

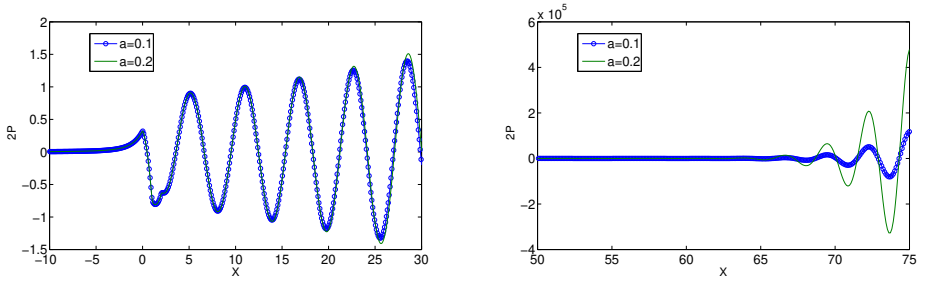

(a) (b)

Figure 5: Results for $Q(T) = -(1 - e^{-aT^2}) \sin \omega_0 T$ with $a = 0.01$ and $a = 0.04$. Results for $\omega_0 = 2.5$ at $t = (K + \frac{1}{4})T_{period}, K = 9$.

1. Supplementary material: Grid independent results and alternative numerical formulation

In order to further validate the above results, we tried a different numerical method to solve the initial-vaue problem. In conducting tests with this new approach it became apparent that the difficulties in obtaining resolved results for the wave packet were due to two main reasons. First the earlier computations were performed over a much larger k range and this made it harder to control the growth of the high wavenumber components during the computation. Restricting the range to $|k| \leqslant 2\pi$ helped to moderate this growth. Secondly, the timesteps required for resolving the wave packet need to be much smaller than we had initially used. Also the difficulties were compounded by working with the triangular shaped vibrator as opposed to using the Gaussian shaped vibrator.

In the new approach the equations are reformulated as a first order system of the form

$$M_{ij}\frac{\partial w_j}{\partial T} + \frac{\partial w_i}{\partial Y} = R_i. \quad i,j = 0,1,2,3, \tag{1.1a}$$

where $M_{ij} = 0$ for $(i,j) \neq (2,1)$ and $M_{2,1} = -1$, with

$$\mathbf{R} = (-ikw_1, w_2, ikYq_1 + w_0 + ikw_3, 0)^T. \tag{1.1b}$$

The boundary conditions are expressed as

$$w_0 = w_1 = 0 \quad \text{on} \quad Y = 0, \tag{1.1c}$$

$$w_2 = w_1 - [q(t)h^*(k) + \frac{w_3}{|k|}] = 0 \quad \text{on} \quad Y = Y_\infty. \tag{1.1d}$$

Here $q(t), h^*(k)$ are described in the paper, with $h^*(k)$ being the Fourier transform of the vibrator shape $h(X)$. We tried

$$q(t) = (1 - e^{-at^2})\sin(\omega_0 t)$$

for different values of a as well as $q(t) = \sin(\omega_0 t)$. The equations (1.1) were solved with a Crank-Nicolson second order time differencing scheme, and using Chebychev collocation for the Y dependence. The results from this approach agreed well with the method as described in the main paper. In figure 6 we have shown results for the unstable case with $\omega = 2.5$ using three different timesteps at two instants in time for the Gaussian hump with an impulsive start $q(t) = \sin(\omega_0 t)$. Similar results are available for the other cases considered and demonstrate convergence with decreasing timesteps.

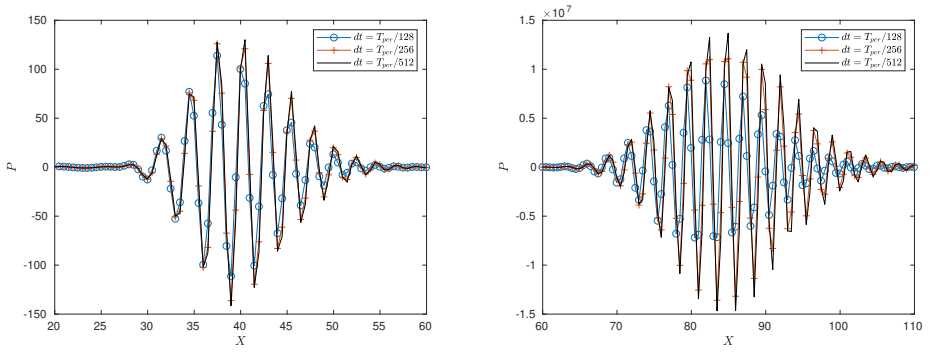

(a) (b)

Figure 6: Results for the pressure P taking timesteps $dt = T_{per}/128$ $dt = T_{per}/256$, $dt = T_{per}/512$ at times (a) $4T_{per}$ and (b) $8T_{per}$ for the unstable case with $\omega = 2.5$ and with 2048 Fourier modes with $|k| < 2\pi$.

2. References

REFERENCES

Terent'ev, E. D. 1984 Linear problem of a vibrator peforming harmonic oscillations at supercritical frequencies in a subsonic boundary layer. *Prikl. Mat. i Mekh.* **48**, 264–272.